

pubs.acs.org/NanoLett Letter

Impact of Electric Field Disorder on Broken-Symmetry States in Ultraclean Bilayer Graphene

Fabian R. Geisenhof, Felix Winterer, Anna M. Seiler, Jakob Lenz, Fan Zhang, and R. Thomas Weitz*



Cite This: Nano Lett. 2022, 22, 7378-7385



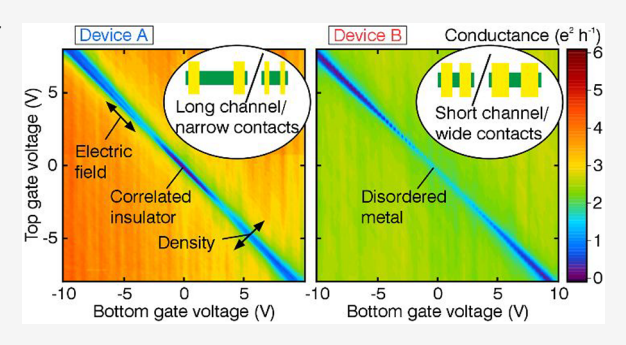
ACCESS I

III Metrics & More

Article Recommendations

Supporting Information

ABSTRACT: Bilayer graphene (BLG) has multiple internal degrees of freedom and a constant density of states down to the charge neutrality point when trigonal warping is ignored. Consequently, it is susceptible to various competing ground states. However, a coherent experimental determination of the ground state has been challenging due to the interaction—disorder interplay. Here we present an extensive transport study in a series of dually gated freestanding BLG devices and identify the layer-antiferromagnet as the ground state with a continuous strength across all devices. This strength correlates with the width of the state in the electric field. We systematically identify electric-field disorder—spatial variations in the interlayer potential difference—as the main



source responsible for the observations. Our results pinpoint for the first time the importance of electric-field disorder on spontaneous symmetry breaking in BLG and solve a long-standing debate on its ground state. The electric-field disorder should be universal to all 2D materials.

KEYWORDS: bilayer graphene, ground state, domain wall, disorder, broken-symmetry state

Bernal bilayer graphene (BLG) has quadratic band touching at the charge neutrality point (CNP) and constant density of states in the single-particle spectrum, when trigonal warping is ignored. This implies that BLG is susceptible to exchange interaction-driven broken-symmetry states.2-13 Such exotic states have been observed at finite magnetic field $B^{3,13-18}$ and, more intriguingly, also in its absence.^{2,6-12} To clearly identify their underlying orders is, however, a long-standing challenge. States at vanishing magnetic field are especially intricate as they are degenerate in mean-field theory^{4,5,19} despite their distinct spin-valley orders. Experimentally, these competing ground states can be characterized by the stability of their resistance against external changes in charge carrier density and electromagnetic field. However, while a vanishing conductance at the CNP suggesting an insulating state 2,6-11 associated with the layer antiferromagnetic (LAF) state^{4,9,10} was found in some devices, finite conductance was seen in others. 6,7,20 Moreover, disparate observations at finite magnetic fields were also reported; for example, a recent study assigned a new quantum Hall state to the transition region between the layer polarized and canted antiferromagnetic $\nu = 0$ states, ²¹ while others did not spot this state.2

Evidently, at both zero and finite magnetic fields, there is no consensus whether the different experimental signatures originate from different interaction-driven states or from disorder. ¹⁹ Charge impurities from substrate or fabrication are one source of disorder. It can be minimized by suspending BLG above a substrate or by encapsulating BLG in hexagonal

boron nitride. However, encapsulation embeds BLG in a dielectric medium with $\varepsilon \sim 3-4$, which substantially reduces the interaction effects compared to the case of suspended devices. Indeed, the spontaneously gapped states have so far not been observed in encapsulated devices. In suspended devices, disorder can be further minimized by current annealing.^{2,22} Another source of disorder are domain walls (DW) that can either naturally occur as stacking defects²³⁻²⁵ or emerge spontaneously due to the interplay between exchange interaction and thermal fluctuation.²⁶ The former, as line defects between AB and BA stacking domains, is not only common in BLG^{24,27} but universal to twisted BLG.²⁸⁻³⁰ Appealingly, these DWs can host topologically protected states.^{23,25,31} The spontaneous DWs are expected to have similar topological properties,²⁶ and they often bind to spatial variation in the potential difference between layers and can proliferate thermally;²⁶ however, they are extremely difficult to identify and control in experiment. Because of these challenges, up to now the impact of DWs on the discussed interactiondriven states and their phase transitions has not been studied

Received: May 25, 2022
Revised: September 13, 2022
Published: September 16, 2022



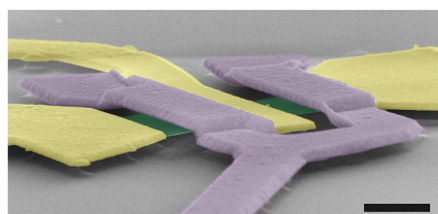


Nano Letters pubs.acs.org/NanoLett Lette

experimentally, although they are expected to alter the quantum transport characteristics in BLG. 26,32

To reveal the origin of the experimental discrepancies in the interaction-driven states at finite and vanishing magnetic fields in BLG, we have carefully examined 11 dually gated suspended BLG devices, of which a representative SEM image is shown in Figure 1a. BLG flakes were first identified by their optical

а



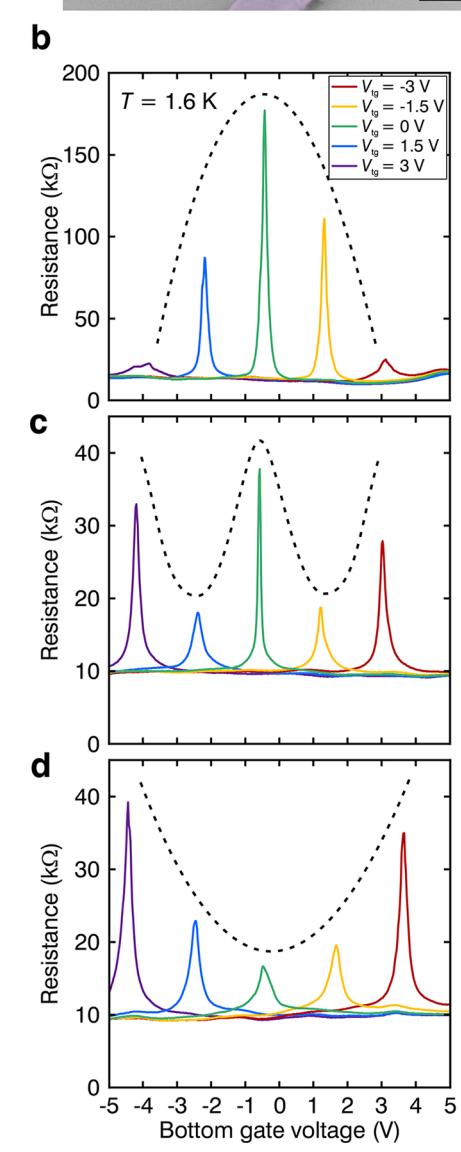


Figure 1. Resistance at charge neutrality in bilayer graphene. a, False-color scanning electron microscope image of a typical suspended bilayer graphene device. Scale bar, 1 μ m. b–d, Resistance as a function of $V_{\rm b}$ measured for a series of $V_{\rm t}$ at T=1.6 K for three different devices. The dashed lines indicate the envelope of the data as a guide to the eye.

contrast and subsequently imaged by scattering-type scanning near-field optical microscopy^{23,27} (s-SNOM) to detect stacking DWs within the flakes (Figure S1). Two out of the 11 devices investigated show clearly pronounced DWs. After fabrication, we performed multiple cycles of current annealing at a temperature of $T=1.6~{\rm K}$ in a dilution refrigerator until a saturation of the current was visible (Figure S2).

We first focus on the comparison of different devices with respect to their behavior at B=0. After current annealing, already at T=1.6 K, bottom gate voltage $V_{\rm b}$ sweeps at various fixed top gate voltages $V_{\rm t}$ reveal differences in the transport signature of the devices (Figure 1b–d). For example, the resistance at the CNP can be very high (>150 k Ω) and decreases with increasing $V_{\rm t}$ (Figure 1b), can be quite low (<20 k Ω) and increases with $V_{\rm t}$ (Figure 1d), or can lie in between these two extremes (Figure 1c). Similar behavior has been described in the literature before 2,6-11,20 and led to a lively debate on the competing ground states and concomitant experimental signatures (e.g., the presence or absence of a gap or edge states).

To gain more insight into the different experimental signatures at the CNP, we mapped the full bottom and top gate voltage range at the base temperature of our cryostat, T <10 mK (Figure 2a). Notably, in 10 out of the 11 devices an insulating state appears at the CNP, while only one device remains metallic. In the following, we will discuss the two most extreme devices, A and B, in which the insulating state is dominant and absent, respectively. For further analysis, we transform V_b and V_t to the perpendicular electric field E and the charge carrier density.n¹² Figure 2b shows the E dependence of the resistance at n = 0, where device A shows the insulating state^{2,6-11} with a resistance of several 100 k Ω around E = 0. According to its signatures, we identify the insulating state as the interaction-driven LAF state^{4,9,10} (see Supplementary Note). Examining the magnitude of the conductance at the CNP, σ_{CNP} , and the width of the spontaneously gapped state in the electric field, $\Delta E^{\rm SP}$, as functions of the temperature reveals an activated T dependence of $\sigma_{\rm CNP}$ and concomitantly an increase of $\Delta E^{\rm SP}$ with decreasing T, as can be observed in device A (see Figure 2c). Moreover, we can see that $\sigma_{\rm CNP}$ and $\Delta E^{\rm SP}$ correlate with the critical temperature across four devices (see Figure S3). We conclude that smaller $\sigma_{
m CNP}$ and larger $\Delta E^{
m SP}$ indicate a more pronounced LAF state and decreasing temperature strengthens this spontaneously gapped state.^{2,7} On the contrary, in device B the resistance monotonically increases with E (Figure 2b), and no significant temperature dependence of σ_{CNP} is observed (Figure 2c). Hence, the spontaneously gapped state is absent, even for T < 10 mK. (We note in passing that we also see a nonmonotonic behavior in the magnetic field of the conductance in device A, which could indicate the transition from the LAF state at B = 0 to the canted antiferromagnetic state at finite B and differences between their edge transport;³³ see Figure S4). In the literature, distinct observations have been made, such as an insulating state^{2,8-11} associated with the LAF state,⁵ a finite conductance,²⁰ or even a bimodal distribution of conductivities at charge neutrality. 6,7 Across our investigated devices, however, we observe continuous distributions of $\sigma_{\rm CNP}$ and $\Delta E^{\rm SP}$ both at T < 10 mK and T = 1.6K (Figure 2d), suggesting a continuous variation of the strength of the LAF state. Our analysis in the remainder of the manuscript is dedicated to deciphering the origin of these distributions.

Nano Letters pubs.acs.org/NanoLett Letter

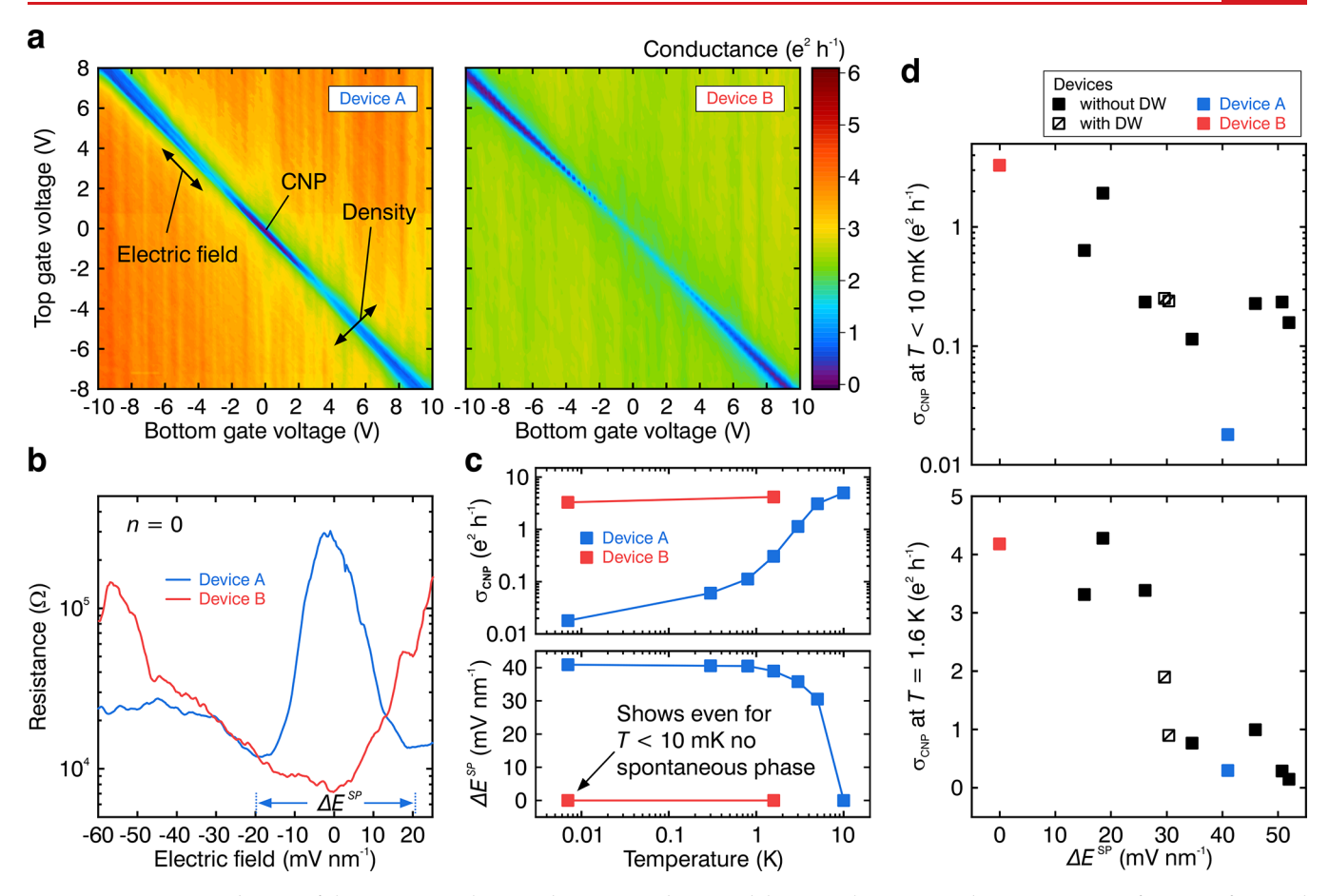


Figure 2. Presence or absence of the spontaneously gapped LAF ground state in bilayer graphene. a, Conductance map as a function of top and bottom gate voltages for devices A and B. b, Trace of the resistance at charge neutrality as a function of E for devices A (blue) and B (red). The electric field range of the insulating spontaneous state is indicated by $\Delta E^{\rm SP}$. c, Conductance at the charge neutrality point $\sigma_{\rm CNP}$ (top) as well as $\Delta E^{\rm SP}$ (bottom) for various temperatures for devices A (blue) and B (red). d, $\sigma_{\rm CNP}$ measured at T < 10 mK (top) and T = 1.6 K (bottom) as a function of $\Delta E^{\rm SP}$ for all measured devices. Devices with (without) a stacking domain wall within the channel are shown with open (solid) squares. Device A (B) is shown in blue (red).

A first possible cause for the observed distribution of σ_{CNP} could be uncontrollable variations in sample fabrication. Such fluctuations of process contaminants are, however, very unlikely since we processed all our devices in the same way. Moreover, we have even found different types of gate dependency when measuring two neighboring contact pairs sharing the same flake, while we have identified similar behavior for two independently processed flakes. A second possible explanation could be the presence of uniaxial strain. However, strain neither opens a spontaneous gap⁸ nor broadens quantum Hall transitions. In fact, to apply substantial uniaxial strain, a special effort is often needed,³⁴ which is not our current case. A third possible reason could be the presence of structural DWs. Such DWs have previously been held responsible for unusual conduction behavior close to the CNP.³⁵ Our experiments, however, demonstrate that DWs are not the cause for suppressing the interaction-driven insulating ground state, since the two devices with DWs show an intermediate strong LAF state, which is consistent with recent experiments revealing that even in the extreme case when a stacking DW directly connects the contacts, the LAF state can still be present.³¹ The arguments hold only with the assumption that the DWs remain stable and do not move during current annealing. Recent literature, however, showed that such stacking DWs can be mobile at high temperatures,²⁴

and even the formation of new stacking boundaries during current annealing resulting in a finite or vanishing conductance at the CNP has been reported.³⁵ To clarify the behavior of stacking DWs under processing and device cleaning, we have conducted a set of test measurements. Since near-field microscopy is impossible to conduct for our dually gated devices, the tests were made on BLG flakes on a substrate without a top gate. At first, we examined the stability of stacking DWs during the fabrication of contacts: in contrast to multilayer graphene,³⁶ they appeared stable and immobile in BLG during processing, verified by their presence prior to and after processing (see Figure S5). This observation is consistent with the prediction that AB and BA stackings are energetically equivalent²⁴ and consequently—unlike DWs between ABC and ABA stacks^{36,37}—there should be no driving force for DW movement by the strain induced during processing. Second, contacted flakes with stacking DWs between the contacts were annealed at large currents and reinvestigated subsequently with near-field microscopy (see Figure S6). We did not observe any systematic movement of the stacking DWs or any development of new ones. We conclude that current annealing and processing do not create, remove, or move stacking DWs systematically. The observed stability implies that two of the investigated devices did indeed have a DW each, which neither

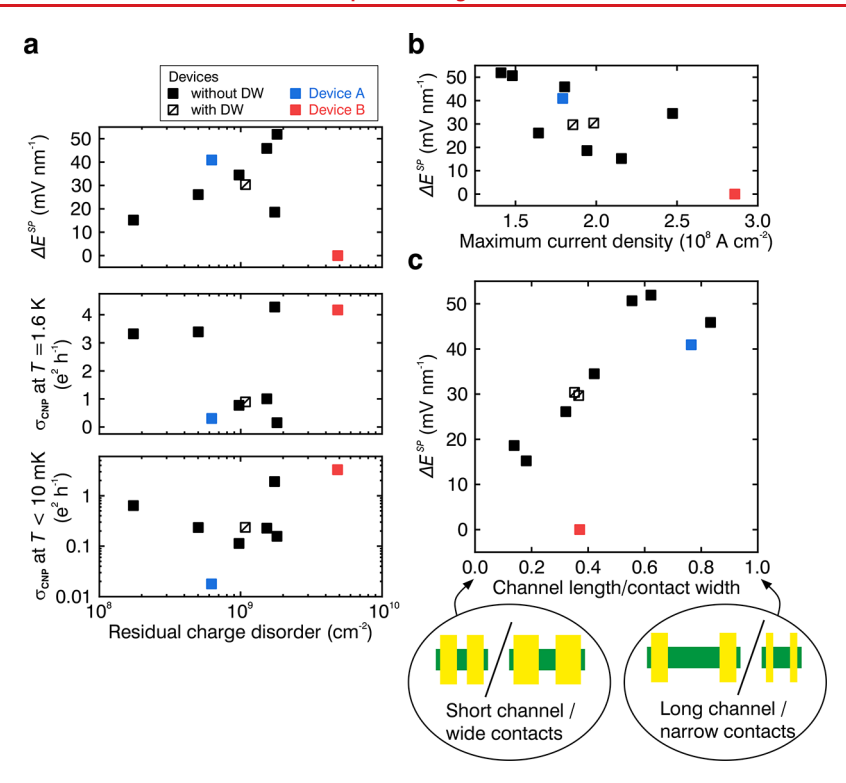


Figure 3. Role of disorder and annealing on the emergence of the gapped LAF ground state in bilayer graphene. a, $\Delta E^{\rm SP}$ and $\sigma_{\rm CNP}$ at T < 10 mK and T = 1.6 K as functions of the residual charge disorder shown for nine devices. b, $\Delta E^{\rm SP}$ as a function of the maximum current density $J_{\rm max}$ applied during the current annealing procedure shown for nine devices. c, $\Delta E^{\rm SP}$ plotted versus the ratio of channel length and contact width of the corresponding device. The schematics in the bottom illustrate the ratio, with the contacts shown in yellow and the bilayer graphene flakes in green.

systematically alters the conductivity of the ground state nor explains the observed continuous spectrum of behavior.

Another possible explanation could be the residual charge disorder in BLG devices. It is often assumed that disorder can be removed via current annealing to a device-independent minimum. Hence, we should be able to clean all devices such that they have similarly low conductance. This is, however, at odds with our experimental findings. Even though we can identify that σ_{CNP} depends on the cleanliness of the device (i.e., the degree of current annealing) and can be changed by more than 1 order of magnitude by further annealing, the overall transport signature (i.e., the monotonic or nonmonotonic behavior of the E dependence of conductance that indicates the absence or presence of the LAF state) does not change once the CNP lies in the accessible $V_{\rm b}$ range (Figure S7). In other words, the emergence of the spontaneously gapped ground state is independent of the number of current annealing cycles in our experiments. Moreover, in the cleanest state accessible by current annealing (i.e., when a current saturation is visible³⁸), $\Delta E^{\rm SP}$ and $\sigma_{\rm CNP}$ do not systematically depend on the residual charge disorder across all devices, which is in general very low in all ultraclean devices (Figure 3a). Therefore, residual charge disorder cannot be the cause, and current annealing itself does not have any effect on the overall transport signatures (Figure S7).

Nonetheless, the current density required to observe saturation during annealing, $J_{\rm max}$, varies significantly in the range of $1.4-2.9\times 10^8$ A cm⁻² between devices. Moreover, the strength of the spontaneously gapped state, $\Delta E^{\rm SP}$, systematically depends on $J_{\rm max}$ (Figure 3b). Specifically, when a high current density is needed for current saturation, the device shows a weaker (or no) gapped ground state. Intriguingly,

besides residual charge disorder, there is a different type of disorder: ^{39,40} Whereas charge fluctuations produce spatially varying in-plane electric fields that lead to charge puddles, ³⁹ i.e., residual charge disorder, charge imbalance between the two layers creates spatially varying out-of-plane electric fields, i.e., electric field disorder. ^{39,40} Moreover, the two types of disorder are most likely uncorrelated. ³⁹

One may wonder from where the electric field disorder originates and why it is not removed during annealing. During the current annealing procedure, the heat generated by the electric current leads to partial evaporation and redistribution of contaminants to colder parts of the devices,³⁸ which in our experiments are the contacts. During fabrication the top layer is exposed to a resist, whereas the bottom layer is in contact with residues initially present on the SiO₂ surface. Hereby, current annealing is more likely to redistribute contaminants within each layer toward the contacts, instead of between the two layers, and we expect the electric field disorder to depend on the device geometry. This hypothesis is ready to be tested by our large number of devices with varying geometries. Indeed, $\Delta E^{\rm SP}$ scales with the ratio of channel length to contact width, as shown in Figure 3c. Evidently, the shorter the graphene channel and/or the wider the contacts, the less effective the current annealing procedure, i.e., the more current is needed to minimize residual charge disorder, and the more electric field disorder is present. Specifically, devices with shorter channels exhibit higher shares of contaminated regions near the contacts compared to devices with longer channels. Moreover, the contacts act as heat sinks, 38 and their widths determine the cooling effectiveness during current annealing, i.e., the wider the contacts the more likely the movement of contaminations toward them. Hence, electric field disorder is

Nano Letters pubs.acs.org/NanoLett Letter

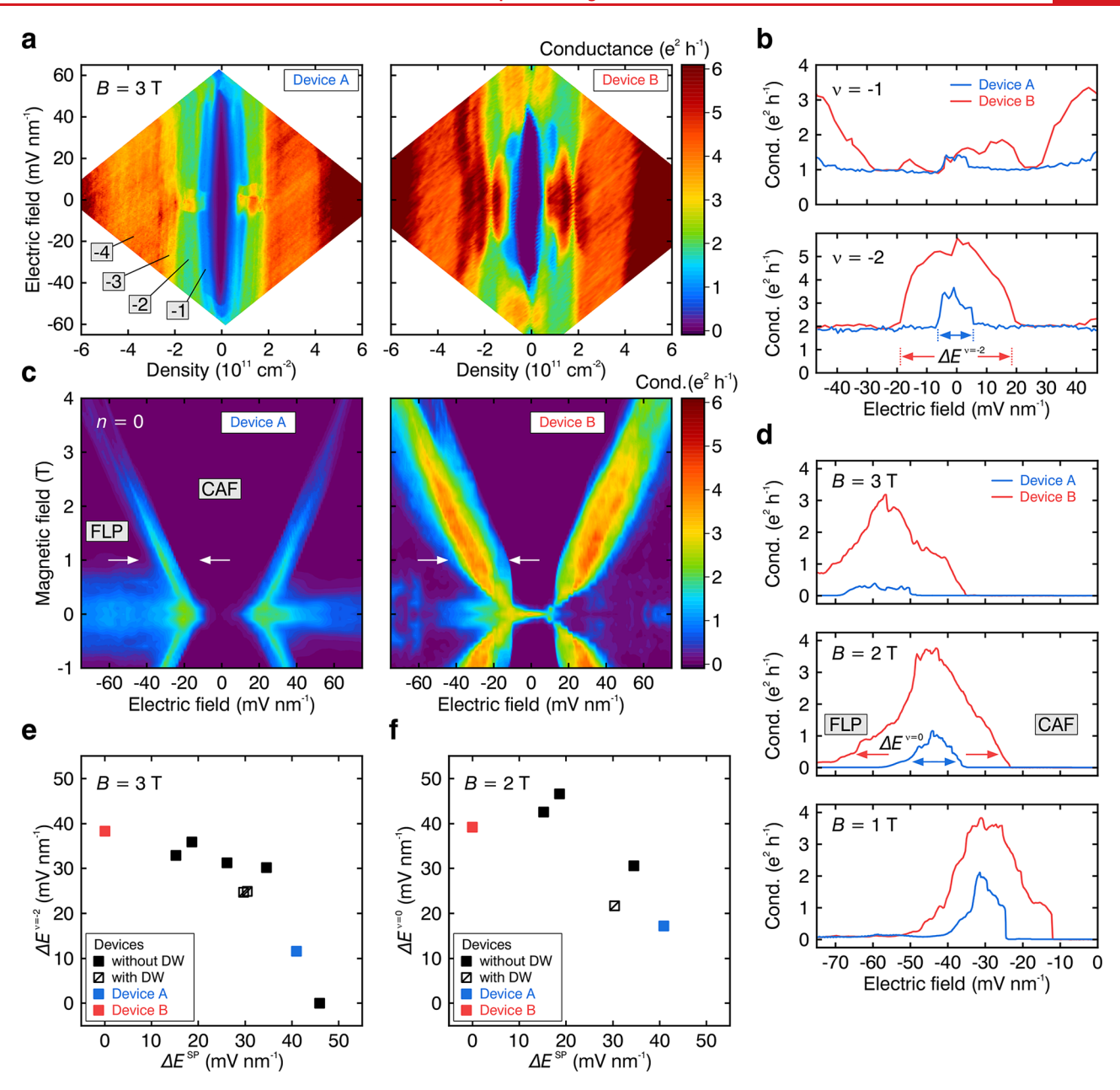


Figure 4. Phase transition between broken-symmetry quantum Hall states and distinct $\nu=0$ states in bilayer graphene. a, Maps of conductance as a function of E and n at B=3 T for devices A and B. b, Line traces of the conductance taken at B=3 T and constant filling factors $\nu=-1$ and -2 as a function of E for devices A (blue) and B (red). The width of the phase transition between $\nu=-2$ states of opposite layer polarization in electric field ($\Delta E^{\nu=-2}$) is indicated. c, Maps of conductance as a function of E and E at zero charge carrier density for devices A and B. The first-order phase transition between the canted antiferromagnetic (CAF) and the fully layer polarized (FLP) states is characterized by a region with increased conductance, indicated by the white arrows. d, Line traces across the $\nu=0$ phase transition at negative electric fields for E=1, E=1, and E=1, E=1 as a function of E=1 and E=1 as a function of E=1 and E=1 as a function of E=1 as a function of E=1 as a function of E=1 and E=1 are E=1 as a function of E=1 and E=1 are E=1 as a function of E=1 and E=1 are E=1 and E=1 are E=1 as a function of E=1 and E=1 are E=1 and

primarily present in devices with short channels and wide contacts. Its presence allows for the formation of domains of competing spontaneously gapped states other than a uniform LAF state²⁶ within a device. Spontaneous DWs separating these domains are known to carry gapless edge modes.²⁶ These can explain the observation of finite $\sigma_{\rm CNP}$ and small $\Delta E^{\rm SP}$.

An estimate of the upper bound of the electric field disorder that completely suppresses the LAF state can be half of $\Delta E^{\rm SP}$ in the cleanest device, namely, ~25 mV nm⁻¹. This corresponds to a charge imbalance of about 1.4×10^{11} cm⁻² in device B,

which is surprisingly large given that the charge disorder is an order of magnitude smaller (Figure 3a). However, the critical disorder strength could be much weaker, as the domain walls between LAF/FLP states are expected to proliferate at the critical point (just like at the critical temperature²⁶). Moreover, the two types of disorder are uncorrelated.³⁹

To find more proof of electric field disorder, we have conducted magneto-transport measurements, since the formation of domains is expected to impact transitions between broken-symmetry quantum Hall states.³² The conductance as a

Nano Letters pubs.acs.org/NanoLett Letter

function of n and E at B = 3 T for devices A and B are shown in Figure 4a (see Figure S8 for data at 1.5 T). Although both devices show the full splitting of the lowest Landau level octet, major differences in the appearance of the $\nu = \pm 1$ and ± 2 states arise. In particular, transitions to the layer polarized ν = ± 1 and ± 2 states around zero electric field can be identified as regions of increased conductance (see Figure 4a,b), as observed previously.^{2,8,17,41} In general, if electric field disorder is strong, around zero electric field, domains of states with opposite layer polarization can be present. Moreover, DWs separating these domains can host one-dimensional conducting states, ^{26,32} increasing the conductance. Whereas the transition regions are narrow in electric field in device A, in device B they are drastically extended and feature enhanced conductance, consistent with many domains and consequently a network of conducting DW states present. Generally, the more domains of states with different layer polarization within a device occur, the more DW states contribute to the charge transport and the more electric field that is needed to uniformly favor a layerpolarized state. On a broader basis, we take the extent of the region of increased conductance in electric field for the $\nu = -2$ state $(\Delta E^{\nu=-2})$ as an indication for the density of conductive DWs and plot it as a function of the width of the LAF ground state in the electric field ΔE^{SP} for several devices (Figure 4e). Systematically, the devices with larger $\Delta E^{\nu=-2}$ also have weaker LAF states at B = 0, consistent with the relevance of the electric field disorder with a concomitant formation of domains in both states. This correlation further corroborates our findings and their explanation at zero magnetic field. Worth mentioning is that these phase-transition regions vanish for very high magnetic fields, since additional layer-balanced, spinpolarized $\nu = \pm 1$, ± 2 states emerge around zero electric field. 17,18

Finally, we turn to another electric-field induced quantum phase transition between two $\nu = 0$ states,³ the canted antiferromagnetic (CAF) phase at low electric fields and the fully layer polarized (FLP) phase at high electric fields. Conductance maps as functions of the applied electric and magnetic fields at zero density are shown for devices A and B in Figure 4c. We find the two $\nu = 0$ insulating states separated by a region with increased conductance, as reported in the literature. 2,3,21 This first order phase transition has a slope in the E-B plane. By taking line traces along negative E at specific B (Figure 4d), one can clearly reveal differences between device A, which displays a sharper transition, and device B, where the phase transition not only has a higher conductance but also extends over a wider range of electric field $\Delta E^{\nu=0}$. Although a recent study attributed the broad transition to the emergence of a new phase,²¹ our data is consistent with the presence of electric field disorder causing the formation of multiple domains of CAF and FLP phases in the transition region. 15 DWs separating the layer unpolarized CAF and the FLP states host one-dimensional conducting states^{26,32} and consequently cause an increase in conductance at the transition. The step-like features likely indicate the switching of individual domains (Figure 4d). To correlate this observation with the strength of the spontaneously gapped ground state at B = 0 (i.e., the LAF state), we plot the width of the $\nu = 0$ transition at negative electric field $\Delta E^{\nu=0}$ at B = 2 T versus ΔE^{SP} for six devices (Figure 4f). Again, devices with a more pronounced spontaneous gap at B = 0 also exhibit a narrower transition between the two $\nu = 0$ states, consistent with the detrimental impact of the electric field disorder.

OUTLOOK

Having identified the electric field disorder as the source for creating domains of different spontaneously gapped ground states at zero magnetic field and broadening the electric fieldinduced phase transitions both at zero magnetic field and in the quantum Hall ferromagnetic regime in BLG poses interesting questions for future investigations. How can one fabricate noninvasive contacts in suspended devices beyond the existing four-terminal ones?⁴² How does the electric field disorder impact the thermal proliferation of spontaneous DWs²⁶ in suspended devices? How does the electric field disorder address the interplay between trigonal warping and Coulomb interaction and the resulting cascade of correlated phases, including fractional metals 13,43,44 and Wigner crystals?¹³ Finally, we note that the existence of electric field disorder should be universal to all 2D materials, and its unique impacts await exploration.

ASSOCIATED CONTENT

Supporting Information

The Supporting Information is available free of charge at https://pubs.acs.org/doi/10.1021/acs.nanolett.2c02119.

Methods used for sample fabrication and characterization, a Supplementary Note with the discussion about the layer antiferromagnetic state, scanning near-field optical microscopy images of the 11 devices (Figure S1), current annealing procedure and the appearance of fractional quantum Hall states (Figure S2), correlation among $\sigma_{\rm CNP}$, $\Delta E^{\rm SP}$, and the critical temperature of the spontaneous ground phase (Figure S3), behavior of the LAF phase with increasing magnetic field (Figure S4), stability of stacking domain walls during processing (Figure S5), stability of stacking domain walls during current annealing (Figure S6), stability of the quantum transport signatures during multiple current annealing cycles (Figure S7), and behavior of the quantum Hall states at B=1.5 T (Figure S8) (PDF)

AUTHOR INFORMATION

Corresponding Author

R. Thomas Weitz — Physics of Nanosystems, Department of Physics, Ludwig-Maximilians-Universität München, Munich 80539, Germany; Center for Nanoscience (CeNS), Munich 80799, Germany; Munich Center for Quantum Science and Technology (MCQST), Munich 80799, Germany; 1st Physical Institute, Faculty of Physics, University of Göttingen, Göttingen 37077, Germany; orcid.org/0000-0001-5404-7355; Email: thomas.weitz@uni-goettingen.de

Authors

Fabian R. Geisenhof – Physics of Nanosystems, Department of Physics, Ludwig-Maximilians-Universität München, Munich 80539, Germany; orcid.org/0000-0002-3623-1906

Felix Winterer — Physics of Nanosystems, Department of Physics, Ludwig-Maximilians-Universität München, Munich 80539, Germany; orcid.org/0000-0002-8344-1615

Anna M. Seiler – Physics of Nanosystems, Department of Physics, Ludwig-Maximilians-Universität München, Munich 80539, Germany; 1st Physical Institute, Faculty of Physics, University of Göttingen, Göttingen 37077, Germany Jakob Lenz – Physics of Nanosystems, Department of Physics, Ludwig-Maximilians-Universität München, Munich 80539, Germany

Fan Zhang – Department of Physics, University of Texas at Dallas, Richardson, Texas 75080, United States;

orcid.org/0000-0003-4623-4200

Complete contact information is available at: https://pubs.acs.org/10.1021/acs.nanolett.2c02119

Author Contributions

F.R.G. fabricated the devices and conducted the measurements. F.R.G. and R.T.W. analyzed the data. F.Z. contributed the theoretical part. All authors discussed and interpreted the data. R.T.W. supervised the experiments and the analysis. The manuscript was prepared by F.R.G., F.Z., and R.T.W with input from all authors.

Notes

The authors declare no competing financial interest.

ACKNOWLEDGMENTS

R.T.W. and F.R.G. acknowledge funding from the Center for Nanoscience (CeNS) and by the Deutsche Forschungsgemeinschaft (DFG, German Research Foundation) under Germany's Excellence Strategy EXC-2111-390814868 (MCQST). F.Z. acknowledges support from the Army Research Office under Grant No. W911NF-18-1-0416 and the National Science Foundation under grant numbers DMR-1945351 through the CAREER program, DMR-2105139 through the CMP program, and DMR-1921581 through the DMREF program. We also thank Y.C. Durmaz, F. Keilmann, and T.D. Gokus for experimental assistance with the near-field optical microscopy measurements.

REFERENCES

- (1) McCann, E.; Fal'ko, V. I. Landau-Level Degeneracy and Quantum Hall Effect in a Graphite Bilayer. *Phys. Rev. Lett.* **2006**, 96, 086805.
- (2) Weitz, R. T.; Allen, M. T.; Feldman, B. E.; Martin, J.; Yacoby, A. Broken-Symmetry States in Doubly Gated Suspended Bilayer Graphene. *Science* **2010**, *330*, 812–816.
- (3) Maher, P.; Dean, C. R.; Young, A. F.; Taniguchi, T.; Watanabe, K.; Shepard, K. L.; Hone, J.; Kim, P. Evidence for a spin phase transition at charge neutrality in bilayer graphene. *Nat. Phys.* **2013**, *9*, 154–158
- (4) Zhang, F.; Jung, J.; Fiete, G. A.; Niu, Q.; MacDonald, A. H. Spontaneous Quantum Hall States in Chirally Stacked Few-Layer Graphene Systems. *Phys. Rev. Lett.* **2011**, *106*, 156801.
- (5) Zhang, F. Spontaneous chiral symmetry breaking in bilayer graphene. *Synth. Met.* **2015**, *210*, 9–18.
- (6) Freitag, F.; Trbovic, J.; Weiss, M.; Schönenberger, C. Spontaneously Gapped Ground State in Suspended Bilayer Graphene. *Phys. Rev. Lett.* **2012**, *108*, 076602.
- (7) Bao, W.; Velasco, J.; Zhang, F.; Jing, L.; Standley, B.; Smirnov, D.; Bockrath, M.; MacDonald, A. H.; Lau, C. N. Evidence for a Spontaneous Gapped State in Ultraclean Bilayer Graphene. *Proc. Natl. Acad. Sci. U.S.A.* **2012**, *109*, 10802–10805.
- (8) Velasco, J.; Jing, L.; Bao, W.; Lee, Y.; Kratz, P.; Aji, V.; Bockrath, M.; Lau, C. N.; Varma, C.; Stillwell, R.; Smirnov, D.; Zhang, F.; Jung, J.; MacDonald, A. H. Transport Spectroscopy of Symmetry-Broken Insulating States in Bilayer Graphene. *Nat. Nanotechnol.* **2012**, *7*, 156–160
- (9) Veligura, A.; van Elferen, H. J.; Tombros, N.; Maan, J. C.; Zeitler, U.; van Wees, B. J. Transport Gap in Suspended Bilayer Graphene at Zero Magnetic Field. *Phys. Rev. B* **2012**, *85*, 155412.

- (10) Freitag, F.; Weiss, M.; Maurand, R.; Trbovic, J.; Schönenberger, C. Spin symmetry of the bilayer graphene ground state. *Phys. Rev. B* **2013**, *87*, 161402.
- (11) Nam, Y.; Ki, D.-K.; Soler-Delgado, D.; Morpurgo, A. F. A Family of Finite-Temperature Electronic Phase Transitions in Graphene Multilayers. *Science* **2018**, *362*, 324–328.
- (12) Geisenhof, F. R.; Winterer, F.; Seiler, A. M.; Lenz, J.; Xu, T.; Zhang, F.; Weitz, R. T. Quantum Anomalous Hall Octet Driven by Orbital Magnetism in Bilayer Graphene. *Nature* **2021**, *598*, 53–58.
- (13) Seiler, A. M.; Geisenhof, F. R.; Winterer, F.; Watanabe, K.; Taniguchi, T.; Xu, T.; Zhang, F.; Weitz, R. T. Quantum Cascade of Correlated Phases in Trigonally Warped Bilayer Graphene. *Nature* **2022**, *608*, 298–302.
- (14) Hunt, B. M.; Li, J. I. A.; Zibrov, A. A.; Wang, L.; Taniguchi, T.; Watanabe, K.; Hone, J.; Dean, C. R.; Zaletel, M.; Ashoori, R. C.; Young, A. F. Direct Measurement of Discrete Valley and Orbital Quantum Numbers in Bilayer Graphene. *Nat. Commun.* 2017, 8, 948.
- (15) Lee, K.; Fallahazad, B.; Xue, J.; Dillen, D. C.; Kim, K.; Taniguchi, T.; Watanabe, K.; Tutuc, E. Bilayer Graphene. Chemical Potential and Quantum Hall Ferromagnetism in Bilayer Graphene. *Science* **2014**, 345, 58–61.
- (16) Li, J.; Tupikov, Y.; Watanabe, K.; Taniguchi, T.; Zhu, J. Effective Landau Level Diagram of Bilayer Graphene. *Phys. Rev. Lett.* **2018**, *120*, 047701.
- (17) Velasco, J.; Lee, Y.; Zhang, F.; Myhro, K.; Tran, D.; Deo, M.; Smirnov, D.; MacDonald, A. H.; Lau, C. N. Competing Ordered States with Filling Factor Two in Bilayer Graphene. *Nat. Commun.* **2014**, *5*, 4550.
- (18) Shi, Y.; Lee, Y.; Che, S.; Pi, Z.; Espiritu, T.; Stepanov, P.; Smirnov, D.; Lau, C. N.; Zhang, F. Energy Gaps and Layer Polarization of Integer and Fractional Quantum Hall States in Bilayer Graphene. *Phys. Rev. Lett.* **2016**, *116*, 056601.
- (19) Zhang, J.; Nandkishore, R.; Rossi, E. Disorder-tuned selection of order in bilayer graphene. *Phys. Rev. B* **2015**, *91*, 205425.
- (20) Mayorov, A. S.; Elias, D. C.; Mucha-Kruczynski, M.; Gorbachev, R. V.; Tudorovskiy, T.; Zhukov, A.; Morozov, S. V.; Katsnelson, M. I.; Fal'ko, V. I.; Geim, A. K.; Novoselov, K. S. Interaction-Driven Spectrum Reconstruction in Bilayer Graphene. *Science* **2011**, 333, 860–863.
- (21) Li, J.; Fu, H.; Yin, Z.; Watanabe, K.; Taniguchi, T.; Zhu, J. Metallic Phase and Temperature Dependence of the N=0 Quantum Hall State in Bilayer Graphene. *Phys. Rev. Lett.* **2019**, 122, 097701.
- (22) Bolotin, K. I.; Sikes, K. J.; Jiang, Z.; Klima, M.; Fudenberg, G.; Hone, J.; Kim, P.; Stormer, H. L. Ultrahigh electron mobility in suspended graphene. *Solid State Commun.* **2008**, *146*, 351–355.
- (23) Ju, L.; Shi, Z.; Nair, N.; Lv, Y.; Jin, C.; Velasco, J.; Ojeda-Aristizabal, C.; Bechtel, H. A.; Martin, M. C.; Zettl, A.; Analytis, J.; Wang, F. Topological Valley Transport at Bilayer Graphene Domain Walls. *Nature* **2015**, *520*, *650*–*655*.
- (24) Alden, J. S.; Tsen, A. W.; Huang, P. Y.; Hovden, R.; Brown, L.; Park, J.; Muller, D. A.; McEuen, P. L. Strain Solitons and Topological Defects in Bilayer Graphene. *Proc. Natl. Acad. Sci. U.S.A.* **2013**, *110*, 11256–11260.
- (25) Zhang, F.; MacDonald, A. H.; Mele, E. J. Valley Chern Numbers and Boundary Modes in Gapped Bilayer Graphene. *Proc. Natl. Acad. Sci. U.S.A.* **2013**, *110*, 10546–10551.
- (26) Li, X.; Zhang, F.; Niu, Q.; MacDonald, A. H. Spontaneous Layer-Pseudospin Domain Walls in Bilayer Graphene. *Phys. Rev. Lett.* **2014**, *113*, 116803.
- (27) Jiang, L.; Shi, Z.; Zeng, B.; Wang, S.; Kang, J.-H.; Joshi, T.; Jin, C.; Ju, L.; Kim, J.; Lyu, T.; Shen, Y.-R.; Crommie, M.; Gao, H.-J.; Wang, F. Soliton-Dependent Plasmon Reflection at Bilayer Graphene Domain Walls. *Nat. Mater.* **2016**, *15*, 840–844.
- (28) Sunku, S. S.; Ni, G. X.; Jiang, B. Y.; Yoo, H.; Sternbach, A.; McLeod, a. S.; Stauber, T.; Xiong, L.; Taniguchi, T.; Watanabe, K.; Kim, P.; Fogler, M. M.; Basov, D. N. Photonic Crystals for Nano-Light in Moiré Graphene Superlattices. *Science* **2018**, 362, 1153—1156.

Nano Letters pubs.acs.org/NanoLett Letter

- (29) Huang, S.; Kim, K.; Efimkin, D. K.; Lovorn, T.; Taniguchi, T.; Watanabe, K.; MacDonald, A. H.; Tutuc, E.; LeRoy, B. J. Topologically Protected Helical States in Minimally Twisted Bilayer Graphene. Phys. Rev. Lett. 2018, 121, 037702.
- (30) Cao, Y.; Fatemi, V.; Fang, S.; Watanabe, K.; Taniguchi, T.; Kaxiras, E.; Jarillo-Herrero, P. Unconventional Superconductivity in Magic-Angle Graphene Superlattices. Nature 2018, 556, 43-50.
- (31) Geisenhof, F. R.; Winterer, F.; Seiler, A. M.; Lenz, J.; Martin, I.; Weitz, R. T. Interplay between topological valley and quantum Hall edge transport. Nat. Commun. 2022, 13, 4187.
- (32) Dhochak, K.; Shimshoni, E.; Berg, E. Spontaneous layer polarization and conducting domain walls in the quantum Hall regime of bilayer graphene. Phys. Rev. B 2015, 91, 165107.
- (33) Kharitonov, M. Edge excitations of the canted antiferromagnetic phase of the ν =0 quantum Hall state in graphene: A simplified analysis. Phys. Rev. B 2012, 86, 075450.
- (34) Ni, Z. H.; Yu, T.; Lu, Y. H.; Wang, Y. Y.; Feng, Y. P.; Shen, Z. X. Uniaxial Strain on Graphene: Raman Spectroscopy Study and Band-Gap Opening. ACS Nano 2008, 2, 2301-2305.
- (35) San-Jose, P.; Gorbachev, R. V.; Geim, A. K.; Novoselov, K. S.; Guinea, F. Stacking Boundaries and Transport in Bilayer Graphene. Nano Lett. 2014, 14, 2052-2057.
- (36) Geisenhof, F. R.; Winterer, F.; Wakolbinger, S.; Gokus, T. D.; Durmaz, Y. C.; Priesack, D.; Lenz, J.; Keilmann, F.; Watanabe, K.; Taniguchi, T.; Guerrero-Avilés, R.; Pelc, M.; Ayuela, A.; Weitz, R. T. Anisotropic Strain-Induced Soliton Movement Changes Stacking Order and Band Structure of Graphene Multilayers: Implications for Charge Transport. ACS Appl. Nano Mater. 2019, 2, 6067-6075.
- (37) Guerrero-Avilés, R.; Pelc, M.; Geisenhof, F. R.; Weitz, R. T.; Ayuela, A. Relative Stability of Bernal and Rhombohedral Stackings in Trilayer Graphene under Distortions. arXiv (Mesoscale and Nanoscale Physics), 2021, 2110.06590v2, http://arxiv.org/pdf/2110. 06590v2 (accessed September 12, 2022).
- (38) Moser, J.; Barreiro, A.; Bachtold, A. Current-induced cleaning of graphene. Appl. Phys. Lett. 2007, 91, 163513.
- (39) Abergel, D. S. L.; Min, H.; Hwang, E. H.; Das Sarma, S. d μ dn in suspended bilayer graphene: The interplay of disorder and band gap. Phys. Rev. B 2011, 84, 195423.
- (40) Rutter, G. M.; Jung, S.; Klimov, N. N.; Newell, D. B.; Zhitenev, N. B.; Stroscio, J. A. Microscopic polarization in bilayer graphene. Nat. Phys. 2011, 7, 649-655.
- (41) Martin, J.; Feldman, B. E.; Weitz, R. T.; Allen, M. T.; Yacoby, A. Local Compressibility Measurements of Correlated States in Suspended Bilayer Graphene. Phys. Rev. Lett. 2010, 105, 256806.
- (42) Ki, D.-K.; Morpurgo, A. F. High-Quality Multiterminal Suspended Graphene Devices. Nano Lett. 2013, 13, 5165-5170.
- (43) Zhou, H.; Holleis, L.; Saito, Y.; Cohen, L.; Huynh, W.; Patterson, C. L.; Yang, F.; Taniguchi, T.; Watanabe, K.; Young, A. F. Isospin Magnetism and Spin-Polarized Superconductivity in Bernal Bilayer Graphene. Science 2022, 375, 774-778.
- (44) de la Barrera, S. C.; Aronson, S.; Zheng, Z.; Watanabe, K.; Taniguchi, T.; Ma, Q.; Jarillo-Herrero, P.; Ashoori, R. Cascade of isospin phase transitions in Bernal-stacked bilayer graphene at zero magnetic field. Nat. Phys. 2022, 18, 771-775.

□ Recommended by ACS

Breaking of Inversion Symmetry and Interlayer Electronic Coupling in Bilayer Graphene Heterostructure by Structural **Implementation of High Electric Displacement Fields**

Marek Kolmer, Michael C. Tringides, et al.

DECEMBER 08, 2022

THE JOURNAL OF PHYSICAL CHEMISTRY LETTERS

RFAD 🗹

Uncovering Topological Edge States in Twisted Bilayer Graphene

Matthieu Fortin-Deschênes, Fengnian Xia, et al.

JULY 28, 2022

NANO LETTERS

READ **C**

Real-Space Mapping of Local Subdegree Lattice Rotations in **Low-Angle Twisted Bilayer Graphene**

Ya-Ning Ren, Lin He, et al.

FEBRUARY 17, 2023

NANO LETTERS

RFAD 17

Moiré Superlattice Effects and Band Structure Evolution in Near-30-Degree Twisted Bilayer Graphene

Matthew J. Hamer, Marcin Mucha-Kruczyński, et al.

JANUARY 24, 2022

ACS NANO

READ **C**

Get More Suggestions >